Effect of magnetite particle size on adsorption and desorption of arsenite and arsenate

S. Yean and L. Cong
Department of Civil and Environmental Engineering, Rice University, Houston, Texas 77005

C.T. Yavuz, J.T. Mayo, and W.W. Yu
Department of Chemistry, Rice University, Houston, Texas 77005

A.T. Kan[a)]
Department of Civil and Environmental Engineering, Rice University, Houston, Texas 77005

V.L. Colvin
Department of Chemistry, Rice University, Houston, Texas 77005

M.B. Tomson
Department of Civil and Environmental Engineering, Rice University, Houston, Texas 77005

(Received 25 April 2005; accepted 2 August 2005)

Numerous studies have examined arsenic adsorption on varying adsorbents including iron oxides, aluminum hydroxides, alumina, and carbon as a means of arsenic removal in drinking water treatments. The objectives of this study were to evaluate the effect of magnetite particle size on the adsorption and desorption behavior of arsenite and arsenate, and to investigate the competitive adsorption between natural organic matter (NOM) and arsenic. Increases in adsorption maximum capacities for arsenite and arsenate were observed with decreasing magnetite particle size. Arsenic desorption is hysteretic, more so with the smaller nanoparticles. Such desorption hysteresis might result from a higher arsenic affinity for magnetite nanoparticles. In the presence of NOM, substantial decrease in arsenic sorption to magnetite nanoparticles was observed. It would be beneficial to thoroughly investigate adsorption and desorption of arsenic on magnetite nanoparticles for further practical purposes.

I. INTRODUCTION

Arsenic-contaminated groundwater, used as drinking water, has been a severe problem in Bangladesh but is also common in United States.[1] Several studies have reported the health hazard due to the chronic exposure to arsenic.[2,3] To address the problem, the World Health Organization (WHO) guideline value and the European maximum permissible concentration (MPC) for arsenic in drinking water are set as 10 μg/l. The United States Environmental Protection Agency[4] also lowered the drinking water standard for arsenic from 50 to 10 μg/l starting January 2006. A variety of arsenic-removal technologies are currently available including coprecipitation, adsorption in fixed-bed filters, membrane filtration, anion exchange, electrocoagulation, and reverse osmosis.[5,6] The focus of research has now shifted to solve the problem using suitable sorbents to achieve a low arsenic level in drinking water for communities with a high raw water arsenic concentration.

Numerous papers have been published, which demonstrate that iron oxides have a high affinity for the adsorption of arsenite and arsenate.[7,8] Although iron oxides have different structures, arsenic adsorption is not affected by their structures.[9] The surface properties of iron oxides are key factors in adsorption on iron oxides. However, the sorption behavior of arsenic is strongly influenced by solution pH and the oxidation state of arsenic. Arsenate is more strongly retained at low pH values,[8] whereas there is conflict about arsenite adsorption versus pH. Increase in arsenite adsorption was observed with increasing pH, with maximum adsorption at approximately pH 9,[8,10] while Dixit and Hering[11] observed that arsenite adsorption was independent of pH in the range of 4 to 10. Arsenic can form inner-sphere bidentate-binuclear complexes with iron oxides.[12–15] Extended x-ray absorption fine structure (EXAFS) spectroscopy as well as Fourier transform infrared (FTIR) spectroscopy[12–15] have provided direct evidence for inner sphere adsorption of arsenite and arsenate on iron oxides. Recently, it has been reported that the As(III) and As(V) form inner sphere complexes on iron oxide as well as hydroxide corrosion products of zerovalent iron, Fe^0.[16] Arsenic adsorption on magnetite resulting from corrosion

[a)]Address all correspondence to this author.
e-mail: atk@rice.edu
DOI: 10.1557/JMR.2005.0403

products of Fe^0 has been studied.[16] When iron oxides dissolve due to changes in pH or in redox conditions, adsorbed arsenic will also dissolve and this has been studied.[17] However, little research has been done on the desorption of adsorbed arsenic. The adsorption and desorption of heavy metals, such as mercury or cadmium from soil, can exhibit considerable hysteresis,[18,19] as well as the desorption of lead and cobalt from hydrous iron oxides.[20] However, the recent investigation using a new sorbent, which contained crystalline and amorphous HFO microparticles in polymer beads demonstrated that both As(III) and As(V) were almost completely desorbed from the sorbent at alkaline pH.[21] Genç-Fuhrman[22] also observed the similar desorption trend. With increasing pH, the desorption rate dramatically enhanced. In this work, the reversibility of arsenic adsorption–desorption from magnetite is evaluated.

Competitive adsorption studies between arsenic and other anions (i.e., phosphate, sulfate, silicic acid, and bicarbonate) have been studied.[10,23–29] Jackson and Miller[24] studied the influence of phosphate concentration (i.e., 0.1 M and 0.5 M NaH_2PO_4) and pH (i.e., pH 3 and pH 7) on arsenic extraction. Extraction efficiencies of arsenate and arsenite from both ferrihydrite and goethite were greater at the higher phosphate concentration (i.e., 0.5 M NaH_2PO_4). Jain and Loeppert[10] observed the suppressed adsorptions of As(III) and As(V) on HFO, in the presence of phosphate. They found that such inhibition highly depended on pH and phosphate concentration. Violante and Pigna[25] reported that arsenate sorption on both goethite and gibbsite decreased with increasing initial molar ratio of phosphate to arsenate up to two (2.0). The previous study of As(III) and As(V) removal kinetics on zerovalent iron showed that phosphate inhibited the greatest removal of both arsenic species.[29] Silicate, chromate, and molybdate also had strong inhibition in arsenic removal rate, followed by carbonate and nitrate.[29] Natural organic matter (NOM), whose concentration commonly is found in natural water between 1 and 50 mg/l as organic carbon, competes with arsenic for sorption sites on hematite.[30] Rapid arsenic sorption to metal oxides was observed;[7,8,31] however, the equilibrium time with NOM-coated hematite was much slower than with hematite and the presence of NOM decreased the extent of arsenic sorption.[30]

Recently, nanomaterials have been of considerable environmental attention due to their small particle size and large surface area. Nanomaterials exhibit different physical, chemical, and biological properties that may not be predictable from observations on larger-sized material, such as monodisperse sizing, freedom from surface defects, and special magnetic and optical properties. Fukushi and Sato[32] showed that surface acidity reaction and surface complexation alter the thermodynamic stability of the underlying iron oxide particles, sometimes in excess of an order of magnitude. For example, with TiO_2, Martra[33] reported that large anatase and nanometer scale TiO_2 exhibit different dominant surface planes leading to very different chemical behavior, surface acidity, and catalytic reactivity. Most nanocrystals were expected to dissolve rapidly in water as predicted from bulk dissolution kinetics per surface area, but often they do not.[34] Redox activity might be similarly diminished. Little is known about the relationship between adsorptive and redox properties of oxides and particle size. Sorbent particles are widely used in separations and analysis of biomolecules; while the challenges faced in that area are distinct from those faced in developing environmental technologies, conceptually the approach and materials are similar.[35–37] Bucak et al.[38] summarized many of the application and theoretical advantages of using nanoparticles for separations, particularly as applied to biomolecular separations. Some of these advantages are directly related to the large and controllable surface areas, but many of the potential advantages are linked to the fundamental nature of a dispersed adsorbent versus a conventional column of fixed packed particles or of a rigid membrane.[38] This dispersed separation avoids many of the classical problems related to plugging and fouling of packed columns and membranes; in a water treatment application, dispersed adsorbents also remove the need for high pressure treatment streams. Moeser et al.[39] showed potential advantages of magnetite nanoparticles in separation because of the extremely small particle size (i.e., ~10 nm) and a large surface area without a high mass-transfer resistance. The high-gradient magnetic separation (HGMS) was able to recover 98% water-based magnetite nanoparticles coated with a bifunctional polymer. In this paper, the adsorption of arsenic to a laboratory prepared monodispersed magnetite nanocrystals is compared with the commercially available magnetite nanomaterials to determine the adsorption of these nanomaterials of different preparations.

II. MATERIALS AND METHODS

A. Materials and mineral sorbents

All chemicals were reagent grade and used without further purification. Solutions were prepared with de-ionized water. Glass volumetric flasks and reaction vessels were cleaned with 10% HNO_3 and rinsed several times with de-ionized water before use. Both As(V) and As(III) stock solutions were prepared by dissolving the arsenic oxides (As_2O_5 and As_2O_3) in de-ionized water, using 4 g/l NaOH. Sorption experiments were conducted with two different sizes of commercially available magnetite with nominal particle sizes of 20 and 300 nm. The 300 nm magnetite sample was purchased from Sigma-Aldrich (Milwaukee, WI). The 20 nm magnetite sample

was from Reade Advanced Materials (Reno, NV). A small amount of monodisperse (11.72 nm) magnetite sample (Houston, TX) was synthesized in the laboratory from iron (III) oxide monohydrate, FeO(OH), by dissolving in oleic acid (90%, technical grade, Aldrich) and heating to elevated temperature (320 °C) in 1-octadecene (90%, technical grade, Aldrich) following the procedure of Yu et al.[40] The as-synthesized magnetite nanocrystals appear as spherical dots with a very narrow size distribution. The synthesized magnetite was then dispersed in water with the aid of a surfactant, Brij 30 (St. Louis, MO), and sonication. The magnetite was then purified by successive washing with water to remove Brij 30. After each washing, the magnetite was separated from supernatant with ultra-high centrifugation at 141 kG. Due to the small quantity of the 11.72 nm magnetite, only limited studies were performed. Surface area was determined by the Brunauer–Emmett–Teller (BET) method using N_2 adsorption onto the magnetite powders using a Micromeritics ASAP 2010 apparatus. Samples were degassed for several hours at 150 °C prior to the N_2 adsorption analysis, which was carried out at liquid-nitrogen temperature (−196 °C). Surface areas were obtained by a multi-point analysis of the volume of nitrogen adsorbed as a function of relative pressure (p/p_0). Transmission electron microscopy (TEM) was performed on a JEOL 2010 apparatus equipped with a JEOL EM21010 (Sunnyvale, CA) single tilt stage. The TEM samples of the 20 and 300 nm magnetite were prepared by evaporating several drops of a dilute ethanol suspension of magnetite powder onto a 300 mesh copper grid. The TEM sample of the 11.72 nm magnetite was prepared by evaporating several drops of the aqueous suspension of magnetite suspension onto a 300 mesh copper grid. The x-ray diffraction (XRD) spectrum of the laboratory prepared magnetite was taken using the Rigaku D-Max 2100 X-ray Diffractometer (Woodlawn, TX). Potentiometric titrations of magnetite suspensions were conducted under nitrogen using a 0.01 mol/l aqueous solution of $NaNO_3$ as the background electrolytes. The two commercially available magnetite samples were used for titrations. The concentration was 5 g/l for 300 nm magnetite nanoparticles and 0.5 g/l for 20 nm magnetite nanoparticles.

B. Sorption isotherms

Sorption isotherms on the magnetite were performed as batch experiments at both environmentally representative and higher concentrations. Arsenic concentrations ranged from 0 to 0.45 mmol/l in a background electrolyte. The concentrations of iron as magnetite were 2.5 g/l for 300 nm magnetite, 0.1 g/l for 20 nm magnetite, and 0.011 g/l for 11.72 nm magnetite nanoparticles. Adsorption studies were obtained at pH of 4.8, 6.1 and 8.0. For the two coarser magnetite samples, the background electrolyte was 0.01 M $NaNO_3$. 2(N-Morpholino)-ethanesulfonate (MES) and Tris at 0.005 M were added as buffers for 6.1 and 8.0 pH experiments, respectively.[41] The pH of the electrolyte was adjusted with a trace amount of HNO_3 or NaOH. For 11.72-nm magnetite nanoparticles, the background electrolyte contained 0.01 M $NaNO_3$ and 0.01 M Tris buffer at pH 8. At the beginning of each experiment, the magnetite was dispersed in solution by sonication in a sonication bath for 10 min. The magnetite electrolyte mixtures were equilibrated on a slowly rotating rack that provided gentle end-over-end tumbling (4 rpm) for 24 h, and centrifuged at 4000 rpm for 30 min. The supernatant solutions were filtered through 0.2 μm Nalgene syringe filters Surfactant-Free Cellulose Acetate (SFCA) for the 20 and 300 nm magnetite samples. A magnetic field column separator was used to separate the solid from liquid phase for 11.72 nm magnetite. The high-gradient magnetic field column separator consisted of S.G. Frantz Canister Separator (Model L-1CN, Trenton, NJ), which had a canister (6.3 mm in width, 25.4 mm in depth, and 222.3 mm in length) and a stainless column (35.3 cm^3). The stainless column was packed with stainless steel wool (~50 μm wire diameter), until the packing volume was 5% of canister (~15 g stainless steel wool). The pH of each solution was measured immediately after sampling. The filtrate was then acidified with 1% nitric acid. All experiments were performed in triplicate, and solutions analyzed for As and Fe by inductively coupled plasma–mass spectroscopy (ICP-MS; Perkin-Elmer Elan 9000, Boston, MA) and inductively coupled plasma (ICP; Perkin-Elmer Optima 4300 DV, Boston, MA), respectively. The detection limit for arsenic using ICP-MS was 0.025 μg/L.

C. Desorption

The 20 and 300 nm magnetite samples were utilized for desorption studies. Desorption was conducted as batch experiments by adding arsenic-free electrolyte to the aliquot, following a 24-h adsorption. Samples were allowed to react for 24 h on a tumbler, centrifuged, and filtered through 0.2 μm Nalgene syringe filters (SFCA) and the pH of each solution was measured immediately, after sampling. The solutions were then acidified and arsenic concentration was measured by ICP-MS. For each adsorption sample, three steps of desorption were performed.

D. Competing anions

Batch experiments were performed in the presence of phosphate and natural organic matter. The Lake Houston water was centrifuged at 5000 rpm for 40 min, and the supernatant was used as the background solution in an adsorption study. Surface water from Lake Houston

(pH = 7.8) contained arsenic (0.0022 mg/l), natural organic matter (16 mg/l as organic carbon), phosphate (0.03 mg/l PO_4^{3-}), and Ca^{2+} (16.2 mg/l). Initial arsenic concentrations in the range of 0–13.5 μmol/l were added to 0.1 g/l 20 nm magnetite nanoparticles. Studies of both As(III) and As(V) sorption on magnetite nanoparticles were performed in 0.01 M $NaNO_3$ and 0.005 M Tris buffer at pH 8 in control experiments. Upon the completion of equilibration for 24 h on the tumbler, samples were filtered through a 0.2 μm Nalgene syringe filters (SFCA) and analyzed for As with ICP-MS (Perkin-Elmer Elan 9000).

III. RESULTS AND DISCUSSION

A. Physical characterization of magnetite samples

In Figs. 1(a)–1(c) are the TEM images of the 300, 20, and 11.72 nm magnetite samples, respectively. The commercially prepared 20 and 300 nm magnetite samples show significant size dispersion and irregular shapes. On the contrary, the TEM image of the laboratory synthesized magnetite particles [Fig. 1(c)] shows highly crystalline monodisperse spherical magnetite nanocrystals. The particle size distribution of the laboratory

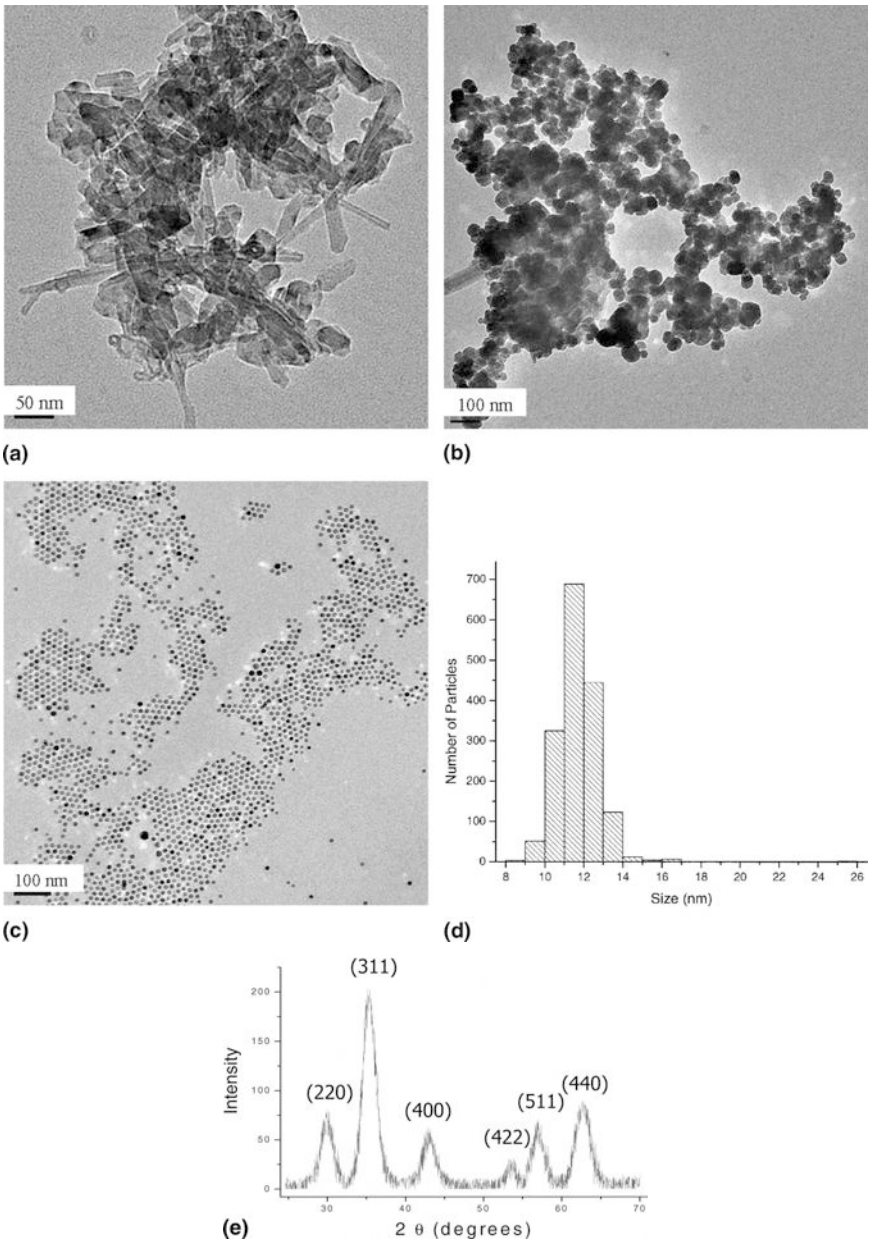

FIG. 1. TEM images of (a) 300 nm magnetite, (b) 20 nm magnetite, (c) 11.72 nm magnetite, (d) histogram of the 11.72 nm magnetite nanocrystals particle sizes, and (d) plot of XRD pattern of 11.72 nm magnetite.

prepared magnetite is shown in Fig. 1(d), which is calculated from the TEM image with a sizing calculation software (ImagePro version 5 of Media Cybernetics, Inc., Silver Spring, MD). The mean particle size was estimated to be 11.72 ± 1.03 nm. In Fig. 1(e) is the XRD spectrum of the laboratory synthesized magnetite, which confirms the magnetite crystal structure.[40] A surface area of 98.8 m^2/g is calculated from the mean particle diameter and magnetite density (5.18 g/cm^3). The BET surface areas of the 20 and 300 nm magnetite samples are 60 and 3.7 m^2/g, respectively. The nominal particle sizes of these two samples were calculated to be 19.3 and 313 nm from BET surface area measurement.

B. Potentiometric titrations of magnetite

The pH versus surface charge σ for 20 and 300 nm magnetite samples is plotted in Fig. 2. Due to a limited quantity of the 11.72 nm magnetite sample, the current potentiometric titration study could not be conducted. The surface charge σ was calculated as a function of pH from potentiometric titration based on Eq. (1)[42]

$$\sigma(C\,m^{-2}) = F(C_A - C_B + [OH^-] - [H^+])a^{-1}S^{-1} \quad , \qquad (1)$$

where F is the Faraday constant (96,485 C/mol), C_A and C_B are the total concentrations of acid and base added, respectively (mol/l), $[H^+]$ is the proton concentration (mol/l) given by $10^{-pH}/\gamma_{H^+}$, $[OH^-]$ is the OH^- concentration (mol/l) given by $10^{-(pKw-pH)}/\gamma_{OH-}$, a is magnetite concentration (g/l), and S is the specific surface area (m^2/g). The titration curves (Fig. 2) are normalized to unit surface area. The point of zero charge (pHpzc) is defined as the pH value at which $\sigma = 0$. Both magnetite samples have the same pzc values of pH 6.8. The results indicated that there was no appreciable difference in the surface acid-base properties of 20 nm magnetite and 300 nm magnetite nanoparticles. The result of pHpzc obtained in this research are close to those from the literature.[43,44]

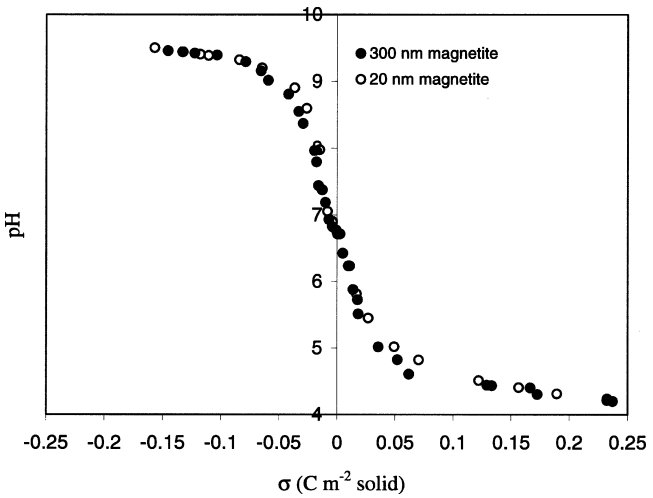

FIG. 2. Potentiometric titration curves for 20 nm magnetite and 300 nm magnetite nanoparticles. For 11.72 nm magnetite nanoparticles, the potentiometric titration study could not be performed due to the limited quantity.

C. Adsorption isotherms

All adsorption data were fitted with the Langmuir isotherm [Eq. (2), solid lines in Fig. 3]:

$$q = \frac{b \cdot q^{max} \cdot C}{1 + b \cdot C} \quad , \qquad (2)$$

where b is the sorption constant related to the adsorption energy (L/μmol) and q^{max} is the maximum sorption capacity of the solid (μmol/g). Both Langmuir parameters were determined by fitting Eq. (2) to experimental adsorption data using the PSI-Plot program (from Poly Software International, Pearl River, NY). In Table I are listed the curve fitted the weight based Langmuir parameters (q^{max}, μmol/g) and the surface-area based Langmuir parameters (q^{max}, μmol/m^2) at 4.8, 6.1, and 8.0 pH.

The adsorption of As(III) to 20 nm magnetite and 300 nm magnetite nanoparticles was not sensitive to pH [Figs. 3(a) and 3(c)]. Due to the pH independence of As(III), only one Langmuir adsorption isotherm was used for all the As(III) data. However, As(III) adsorption maxima to 300 nm magnetite was approximately 18 times less than those of 20 nm magnetite nanoparticles and the surface area differed by a factor of 16; i.e., proportional to surface area. The pH independency of As(III) can be explained by the high pKa value of As(III) (i.e., $pK_{a,1} = 9.22$). Thus, arsenite was present mostly as a neutral species up to pH 8.0. The adsorption of this nonionic form of As(III) to magnetite surface did not change with pH.

The maximum adsorption capacities of As(V) for 20 and 300 nm magnetite decreased with increasing pH [Figs. 3(b) and 3(d)]. The surface of magnetite is positively charged at pH values below 6.8 due to the pzc of magnetite. Thus, stronger As(V) adsorption to magnetite samples was observed at lower pH values. The reduction in As(V) adsorption at high pH (i.e., pH 8) was attributable to the electrostatic repulsion of the negatively charged As(V) species by the negatively charged surface sites. With respect to the effect of magnetite size, both As(III) and As(V) had greater affinities for 20 nm magnetite particles, as indicated by the larger values of q^{max} b products (Table I, Column 8).

At each pH condition, the weight based As(III) and As(V) adsorption capacities (q^{max}, μmol/g) were larger for 20 nm magnetite particles with higher surface area (Table I); however, the surface-area based As(III) and As(V) adsorption capacities (q^{max}, μmol/m^2) were very similar for 20 nm magnetite and 300 nm magnetite nano-

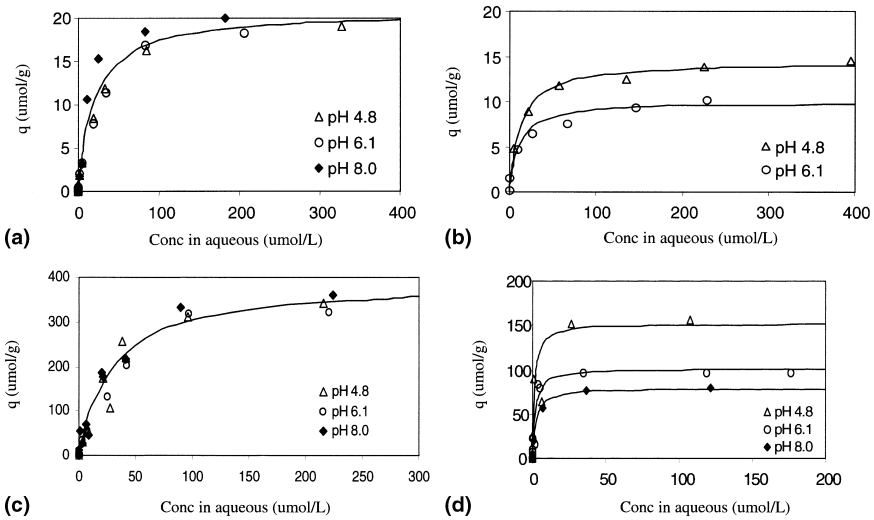

FIG. 3. (a) As(III) adsorption to 300 nm magnetite at pH 4.8, 6.1, and 8.0, (b) As(V) adsorption to 300 nm magnetite at pH 4.8 and 6.1, (c) As(III) adsorption to 20 nm magnetite at pH 4.8, 6.1, and 8.0, and (d) As(V) adsorption to 20 nm magnetite at pH 4.8, 6.1, and 8.0. The solid curves are drawn using the curve-fitted isotherm data in Table I.

TABLE I. Weight based and surface-area based Langmuir adsorption isotherm parameters.

Arsenic	Magnetite	pH	b (L/μmol)	q^{max} (μmol/g)	q^{max}·b (L/g)	q^{max} (μmol/m^2)	q^{max}·b (L/m^2)
As(III)	300 nm	4.8–8.0[a]	0.05	20.8	1.04	5.62	0.28
As(III)	20 nm	4.8–8.0[a]	0.04	388.9	13.98	6.48	0.23
As(III)	11.72 nm	8.0	0.02	1532	31.79	15.49	0.32
		8.0	0.02[b]	1800	37.40	18.22	0.38
As(V)	300 nm	4.8	0.08	14.4	1.12	3.89	0.32
		6.1	0.10	10.0	0.98	2.70	0.26
As(V)	20 nm	4.8	0.82	152.3	125.49	2.54	2.09
		6.1	0.54	101.3	54.71	1.69	0.91
		8.0	0.48	79.4	38.07	1.32	0.63
As(V)	11.72 nm	8.0	0.11	622.7	66.63	6.3	0.67
		8.0	0.11[b]	2300	24.61	23.28	2.49

[a]Arsenite adsorption is independent of pH.
[b]b values for the second maxima were assumed to be the same as that for the first maxima.

particles, but each shows a systematic decrease in q^{max} (μmol/m^2) with increasing pH.

Arsenic adsorption to 11.72 nm magnetite nanoparticles is plotted in Fig. 4. As seen by others,[11] the adsorption isotherm appeared to consist of two Langmuir type isotherms for both As(III) and As(V). At low concentrations [<120 μmol/L As(III) or <50 μmol/L As(V)], the adsorption isotherms can be fitted with simple Langmuir isotherms where maximum adsorption capacities approach 1532 μmol/g for As(III) and 622.7 μmol/g for As(V). This is equivalent to 15.5 and 6.3 μmol/m^2 for As(III) and As(V) or 9.3 and and 3.8 molecules per nm^2 of As(III) and As(V), respectively. The surface-area based arsenic adsorption maxima to 11.72 nm magnetite of the first adsorption maxima are approximately 2.4 and 4.8 times [for As(III) and As(V), respectively] higher than that of the 20 nm magnetite nanoparticles. At high As concentrations [>120 μmol/L As(III) or >50 μmol/L As(V)], the adsorption data deviates from the simple Langmuir isotherm and appears to follow a second Langmuir isotherm. For the second isotherm, the sorption energy (b term) was assumed to be the same as that of the first sorption energy to evaluate the second maximum adsorption capacity. The second maximum adsorption capacities (q^{max}) for As(III) and As(V) were substantially higher, which may be a result of the coprecipitation of As with Fe on the surface.[32,45,46] Our results show that, with 11.72 nm magnetite, the second maximum adsorption capacities are 18 and 24 μmol/m^2 for As(III) and As(V), respectively. This adsorption corresponds to 0.14 and 0.18 mol As/mol Fe in magnetite. Previous studies have shown that for As(V) the adsorption maxima on HFO is approximately 0.25 mol As/mol Fe at pH 4.6 and at pH 8.0.[8,31] Dixit and Hering[11] found

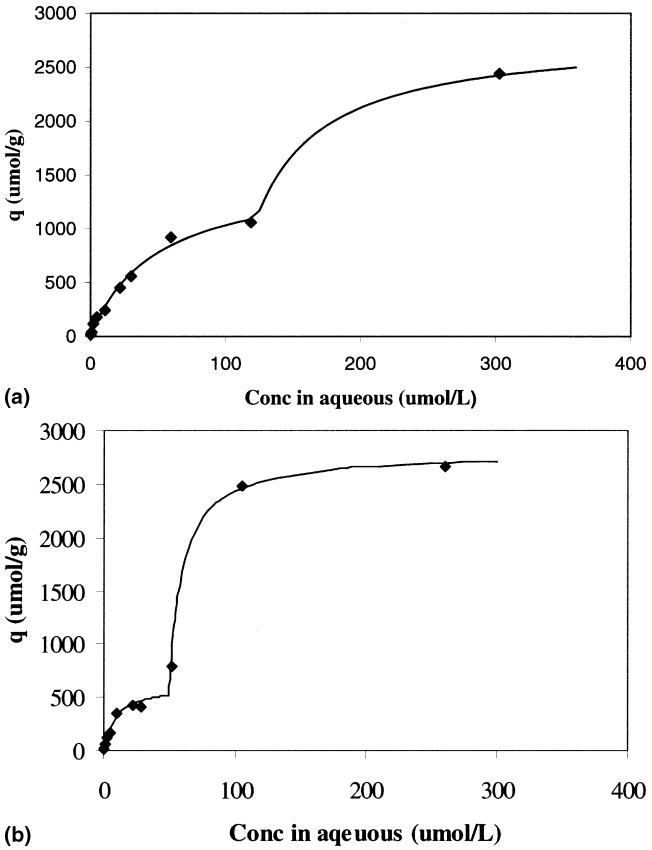

FIG. 4. Plot of the adsorption of As(III) and As(V) to 11.72 nm magnetite at pH 8.0: (a) As(III) to 11.72 nm magnetite and (b) As(V) to 11.72 nm magnetite.

adsorption of 0.24 mol As(V)/mol Fe at pH 4. Raven et al.[8] observed adsorption densities of about 0.6 mol As/mol Fe at 4.6 and 9.2 pH, but this occurred at about 15 mM solution phase arsenic. Surprisingly, even at these very high concentrations, they did not observe a leveling off of the adsorption. Dixit and Hering[11] found a maximum sorption density for As(III) on HFO of 0.31 mol As/mol Fe, which is 2.2 times the amount adsorbed per mole of iron in 11.72 nm magnetite. Consequently, the maximum adsorption densities for 11.72 nm magnetite are less than, but comparable to, the maximum densities reported for high surface area hydrated ferric oxide, even though HFO has a 6-fold larger surface area (i.e., 600 m^2/g).[11,47] Dixit and Hering[11] reported similar maximum sorption capacities for As(III) and As(V) on goethite, which was 0.016 mol As/mol Fe. They also studied the arsenite adsorption on magnetite at pH 8. Their maximum adsorption density for As(III) corresponded to 0.025 mol As/mol Fe. With the specific surface area of their magnetite at 90 m^2/g, the site density appeared to be 2.2 sites/nm^2. In spite of a similar specific surface area, our 11.72 nm magnetite showed approximately 6-fold higher arsenic adsorption capacity for As(III).

D. Desorption

Desorption experiments were then performed on the 20 and 300 nm magnetite nanoparticles to examine the reversibility of the sorption reaction. Desorption was not done with the 11.72 nm magnetite due to limited samples. Desorption hysteresis has been reported for many gas-solid and liquid-solid interactions.[20,21,48–50] Genç-Fuhrman[22] observed that arsenate desorption rate was less than 15% up to pH 8, which indicated that arsenic adsorption on an activated neutralized red mud was irreversible at common environmental pH ranges; however, 40% of arsenic was desorbed at pH 11.6, and desorption rate remarkably increased with increasing pH (>9). Also, DeMarco et al.[21] reported the almost complete desorption of both As(III) and As(V) at alkaline pH (i.e., >pH 11) in a recent study where iron oxide was dispersed in porous polymer beads. In this research, desorption of As(III) and As(V) from 20 and 300 nm magnetite samples was studied to determine the effect of particle size on desorption behavior. In Fig. 5 are plotted the weight based desorption data of As(III) and As(V) from 20 and 300 nm magnetite at pH 6.1. As shown in Figs. 5(a) and 5(c), desorption of both As(III) and As(V) from 300 nm magnetite particles appears to be irreversible. After three steps of desorption, each taking 24 h, only 20–25% of the adsorbed As(III) or As(V) was desorbed from the 300 nm magnetite nanoparticles. Desorption of both As(III) and As(V) from 20 nm magnetite nanoparticles exhibited almost complete desorption hysteresis [Figs. 5(b) and 5(d)]. After three steps of desorption, each taking 24 h, only about 1% of the adsorbed As(III) or As(V) was removed from these magnetite nanoparticles. Similar hysteretic desorption phenomena were observed at pH 4.8 and 8.0. The results indicated that smaller particle size of magnetite has higher adsorption affinity for As(III) and As(V). The 20 nm magnetite offered unique advantages over the 300 nm magnetite on both stronger sorption due to increased surface area and negligible bleed-off at common environmental pH conditions due to desorption hysteresis. Both stronger adsorption and resistant desorption and bleed-off are a significant advantage in water treatment and solid waste disposal.

E. Competitive sorption

In Fig. 6 are plotted the arsenic sorption to 20 nm magnetite nanoparticles in Lake Houston water and 0.01 M $NaNO_3$ electrolyte solution (pH 8.0). Apparently, the sorption of both As(III) and As(V) to magnetite nanoparticles in the Lake Houston water was lower than that in 0.01 M $NaNO_3$ electrolyte. Since the Lake Houston water and laboratory-made water had almost the same pH (7.8 versus 8.0), pH probably was not a factor affecting the difference of arsenic sorption behavior. Previous

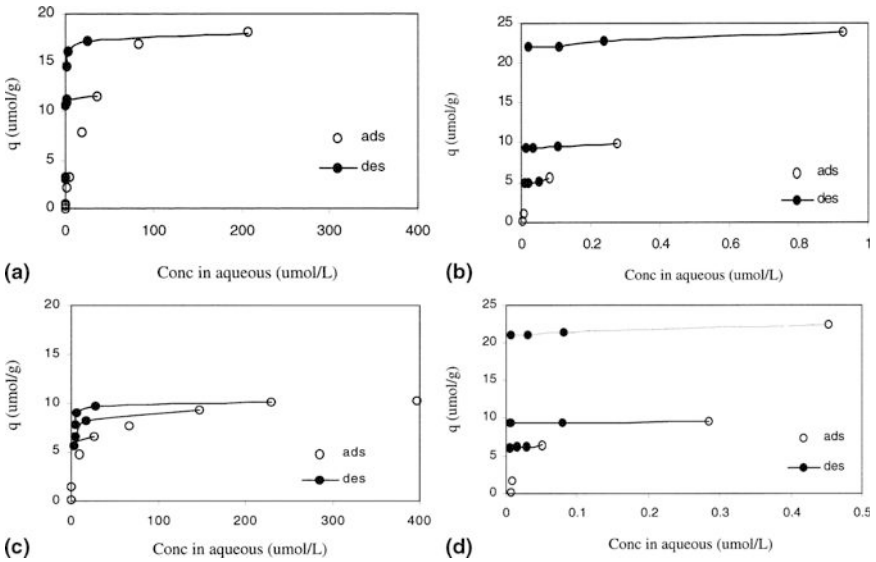

FIG. 5. Plot of the adsorption/desorption of As(III) and As(V) to 300 nm and 20 nm magnetite samples at pH 6.1: (a) As(III) to 300 nm magnetite, (b) As(III) to 20 nm magnetite, (c) As(V) to 300 nm magnetite, and (d) As(V) to 20 nm magnetite. The open symbols are data from adsorption approach and the closed symbols are desorption data for selected adsorption points.

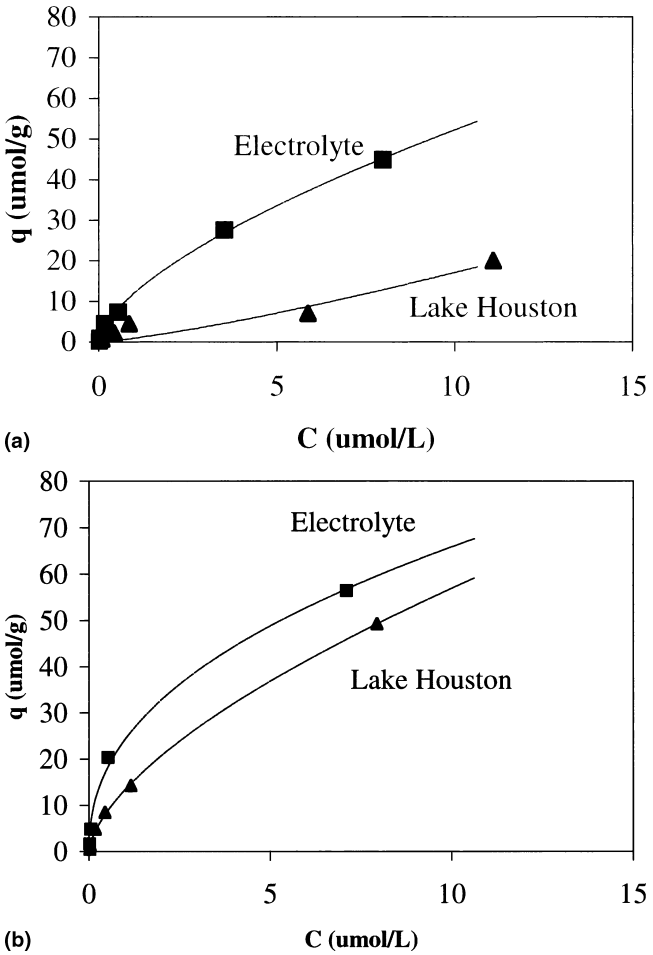

FIG. 6. Plot of (a) As(III) sorption to 20 nm magnetite in Lake Houston water and laboratory-made electrolyte (0.01 M $NaNO_3$, pH 8.0) and (b) As(V) sorption to 20 nm magnetite in Lake Houston water and laboratory-made electrolyte (0.01 M $NaNO_3$, pH 8.0).

research has shown that arsenic sorption to mineral surfaces decreases in the presence of competitive anions such as phosphate, sulfate, nitrate, and molybdate.[10,23–27,29,51] In the Lake Houston water, arsenic was present as 0.0022 mg/l, which is equivalent to approximately 0.03 μmol/l. Compared to arsenic concentrations added for the adsorption studies, the concentration of arsenic present was negligible. After the filtration, iron concentrations ranging from 5 to 27 μg/l were negligible, compared to the initial concentration (i.e., 0.1 g/l). The PO_4^{3-} concentration was found to be 0.03 mg/l, which was negligible compared to NOM concentration (16 mg/l as organic carbon). Therefore, the decreased As adsorption was probably due to the NOM, but other components in the lake water might also be important. NOM in the solution probably competed with As(III) and As(V) species for the surface sites (hydroxyl groups) on magnetite and decreased the sorption of As(III) or As(V) to magnetite surface. The sorption of NOM to magnetite nanoparticles is assumed to be a dynamic interaction of several mechanisms between organic functional groups (mainly COOH and OH) and surface hydroxyl groups including ligand exchange reactions, hydrogen bonding, and electrostatic interactions.

IV. CONCLUSION

Arsenic adsorption maximum capacity and desorption hysteresis were strongly influenced by magnetite particle size. On the basis of surface area, adsorption maximum capacity for both arsenic species was similar for the commercially prepared (20 and 300 nm) magnetite samples. However, the adsorption capacity for both As(III) and

As(V) to laboratory prepared (11.72 nm) magnetite increased significantly compared to the commercially prepared magnetite. This observation may result from more adsorption sites being exposed to arsenic by the 11.72 nm magnetite, which was completely dispersed in solution. We have shown that when prepared in a nanocrystalline form, magnetite can remove two hundred times more arsenic than the larger commercial materials, on a weight percent basis. Regarding desorption, smaller particles tended to show stronger desorption hysteresis, presumably because the binding of the adsorbed arsenic resulted in the formation of highly stable iron-arsenic complexes uniformly over the surface. Thus, once loaded these nanoparticles resist arsenic desorption and bleed-off, a significant advantage in disposal at common environmental pH ranges. Finally, the magnetite particles synthesized in the laboratory tend to have unique magnetic behavior.[52] By carefully optimizing the particle size,[52] highly efficient magnetic separation systems using low field strengths might be used in treatment processes.

ACKNOWLEDGMENTS

We acknowledge the financial support from National Science Foundation through the Center for Biological and Environmental Nanotechnology [EEC-0118007], United States Environmental Protection Agency (US EPA) Office of Research and Development (ORD)/ National Center for Environmental Research (NCER)/ Science to Achieve Result (STAR) program, US EPA Hazardous Substance Research Center/South & Southwest Region, and Rice University Brine Chemistry Consortium of companies: Aramco, Baker-Petrolite, Champion Technologies, Inc., Chevron-Texaco, Inc., Clariant UK Ltd., ConocoPhillips, Inc., Marathon Oil, Nalco, and Occidental Oil and Gas.

REFERENCES

1. M. Bissen and F.H. Frimmel: Arsenic—A review. Part I: Occurrence, toxicity, speciation, mobility. *Acta Hydroch. Hydrob.* **31,** 9 (2003).
2. L.C.D. Anderson and K.W. Bruland: Biogeochemistry of arsenic in natural waters: The importance of methylated species. *Environ. Sci. Technol.* **25,** 420 (1991).
3. W.P. Tseng, H.M. Chu, S.W. How, J.M. Fong, C.S. Lin, and S. Yeh: Prevalence of skin cancer in an endemic area of chronic arsenicism in Taiwan. *J. Nat. Cancer Inst.* **40,** 453 (1968).
4. Clarifications to compliance and new source contaminants monitoring. Assessed on April, 2005. http://www.epa.gov/safewater/ars/arsenic_finalrule.pdf.
5. L.G. Twidwell, J. McCloskey, P. Miranda, and M. Gale: Technologies and potential technologies for removing arsenic from process and mine wastewater, in *Proceedings, Global Symposium on Recycling, Waste Treatment and Clean Technology*, edited by I. Gaballah, J. Hager and R. Solozabal, Editors. (TMS, Warrendale, PA. 1999), pp. 1715–1726.
6. M. Bissen and F.H. Frimmel: Arsenic—A review. Part II: Oxidation of arsenic and its removal in water treatment. *Acta Hydroch. Hydrob.* **31,** 97 (2003).
7. M.L. Pierce and C.B. Moore: Adsorption of arsenite and arsenate on amorphous iron hydroxide. *Water Res.* **15,** 1247 (1982).
8. K.P. Raven, A. Jain, and R.H. Loeppert: Arsenite and arsenate adsorption on ferrihydrite: Kinetics, equilibrium, and adsorption envelopes. *Environ. Sci. Technol.* **32,** 344 (1998).
9. G.Y.J. Onoda and P.L. DeBruyn: Proton adsorption at the ferric oxide/aqueous solution interface. *Surf. Sci.* **4,** 48 (1966).
10. A. Jain and R.H. Loeppert: Effect of competing anions on the adsorption of arsenate and arsenite by ferrihydrite. *J. Environ. Qual.* **29,** 1422 (2000).
11. S. Dixit and J.G. Hering: Comparison of arsenic(V) and arsenic(III) sorption onto iron oxide minerals: Implications for arsenic mobility. *Environ. Sci. Technol.* **37,** 4182 (2003).
12. S. Fendorf, M.J. Eick, and P. Grossl: Arsenate and chromate retention mechanisms on goethite. 1. Surface structure. *Environ. Sci. Technol.* **31,** 315 (1997).
13. A. Manceau: The mechanism of anion adsorption on iron-oxides—Evidence for the bonding of arsenate tetrahedra on free Fe(O,OH)(6) edges. *Geochim. Cosmochim. Acta* **59,** 3647 (1995).
14. X.H. Sun and H.E. Doner: An investigation of arsenate and arsenite bonding structure on goethite by FTIR. *Soil Sci.* **161,** 865 (1996).
15. G.A. Waychunas, B.A. Rea, C.C. Fuller, and J.A. Davis: Surface chemistry of ferrihydrite, Part l. EXAFS studies of the geometry of coprecipitated and adsorbed arsenate. *Geochim. Cosmochim. Acta* **57,** 2251 (1993).
16. B.A. Manning, M.L. Hunt, C. Amrhein, and J.A. Yarmoff: Arsenic(III) and arsenic(V) reactions with zerovalent iron corrosion products. *Environ. Sci. Technol.* **36,** 5455 (2002).
17. S.R. Hinkle and D.J. Polette: *Arsenic in Ground Water of the Willamette Basin, Oregon* (U.S. Geological Survey, Portland, OR, 1999).
18. Y. Gao, R. Wahi, A.T. Kan, J.C. Falkner, V.L. Colvin, and M.B. Tomson: Adsorption of cadmium on anatase nanoparticles-effect of crystal size and pH. *Langmuir* **20,** 9585 (2004).
19. Y. Yin, H.E. Allen, C.P. Huang, and P.F. Sanders: Adsorption/desorption isotherms of Hg(II) by soil. *Soil Sci.* **162,** 35 (1997).
20. C.C. Ainsworth, J.L. Pilou, P.L. Gassman, and W.G. Van Der Sluys: Cobalt, cadmium, and lead sorption on hydrous iron oxide: Residence time effect. *Soil Sci. Soc. Am. J.* **58,** 1615 (1994).
21. M.J. DeMarco, A.K. SenGupta, and J.E. Greenleaf: Arsenic removal using a polymeric/inorganic hybrid sorbent. *Water Res.* **37,** 164 (2003).
22. H. Genç-Fuhrman, J.C. Tjell, and D. McConchie: Adsorption of arsenic from water using activated neutralized red mud. *Environ. Sci. Technol.* **38,** 2428 (2004).
23. C.A.J. Appelo, M.J.J. Van der Weiden, C. Tournassat, and L. Charlet: Surface complexation of ferrous iron and carbonate on ferrihydrite and the mobilization of arsenic. *Environ. Sci. Technol.* **36,** 3096 (2002).
24. B.P. Jackson and W.P. Miller: Effectiveness of phosphate and hydroxide for desorption of arsenic and selenium species from iron oxides. *Soil Sci. Soc. Am. J.* **64,** 1616 (2000).
25. A. Violante and M. Pigna: Competitve sorption of arsenate and phosphate on different clay minerals and soils. *Soil Sci. Soc. Am. J.* **66,** 1788 (2002).
26. B.A. Manning and S. Goldberg: Modeling arsenate competitive adsorption on kaolinite, montmorillonite and illite. *Clays Clay Miner.* **44,** 609 (1996).
27. P.J. Swedlund and J.G. Webster: Adsorption and polymerisation

of silicic acid on ferrihydrite, and its effect on arsenic adsorption. *Water Res.* **33,** 3413 (1999).
28. E. Smith, R. Naidu, and A.M. Alston: Chemistry of inorganic arsenic in soils: II. Effect of phosphorous, sodium, and calcium on arsenic sorption. *J. Environ. Qual.* **31,** 557 (2002).
29. C.M. Su and R.W. Puls: Arsenate and arsenite removal by zerovalent iron: Effects of phosphate, silicate, carbonate, borate, sulfate, chromate, molybdate, and nitrate relative to chloride. *Environ. Sci. Technol.* **35,** 4562 (2001).
30. A.D. Redman, D.L. Macalady, and D. Ahmann: Natural organic matter affects arsenic speciation and sorption onto hematite. *Environ. Sci. Technol.* **36,** 2889 (2002).
31. C.C. Fuller, J.A. Davis, and G.A. Waychunas: Surface-chemistry of ferrihydrite 2. Kinetics of arsenate adsorption and corprecipitation. *Geochim. Cosmochim. Acta* **57,** 2271 (1993).
32. K. Fukushi and T. Sato: Using a surface complexation model to predict the nature and stability of nanoparticles. *Environ. Sci. Technol.* **39,** 1250 (2005).
33. G. Martra: Lewis acid and base sites at the surface of microcrystalline TiO_2 anatase: Relationships between surface morphology and chemical behaviour. *Appl. Catal. Gen.* **200,** 275 (2000).
34. A. Luttge, E.W. Bolton, and A.C. Lasaga: An interferometric study of the dissolution kinetics of anorthite: The role of reactive surface area: in Biogeochemical cycles and their evolution over geologic time. *Am. J. Sci.* **299,** 652 (1999).
35. Z. Bilkova, M. Slovakova, A. Lycka, D. Horak, J. Lenfeld, J. Turkova, and J. Churacek: Oriented immobilization of galactose oxidase to bead and magnetic bead cellulose and poly(HEMA-co-EDMA) and magnetic poly(HEMA-co-EDMA) microspheres. *J. Chromatogr. B Analyt. Technol. Biomed. Life Sci.* **770**(1–2), 25 (2002).
36. Z. Bilkova, M. Slovakova, D. Horak, J. Lenfeld, and J. Churacek: Enzymes immobilized on magnetic carriers: Efficient and selective system for protein modification. *J. Chromatography B* **770,** 177 (2002).
37. W. Sun, F. Khosravi, H. Albrechtsen, L.Y. Brovko, and M.W. Griffiths: Comparison of ATP and in vivo bioluminescence for assessing the efficiency of immunomagnetic sorbents for live Escherichia coli O157: H7 cells. *J. Appl. Microbiol.* **92,** 1021 (2002).
38. S. Bucak, D.A. Jones, P.E. Laibinis, and T.A. Hatton: Protein separations using colloidal magnetic nanoparticles. *Biotechnol. Prog.* **19,** 477 (2003).
39. G.D. Moeser, K.A. Roach, W.H. Green, P.E. Laibinis, and T.A. Hatton: Water-based magnetic fluids as extractants for synthetic organic compounds. *Ind. Eng. Chem. Res.* **41,** 4739 (2002).
40. W.W. Yu, J.C. Falkner, B.S. Shih, and V.L. Colvin: Preparation and characterization of monodisperse PbSe semiconductor nanocrystals in a noncoordinating solvent. *Chem. Mater.* **16,** 3318 (2004).
41. R.G. Bates: *Determination of pH: Theory and Practice* (John Wiley & Sons, New York, 1973).
42. W. Stumm and J.J. Morgan: *Aquatic Chemistry: Chemical Equilibria and Rates in Natural Waters* (Wiley-Interscience, New York, 1995).
43. P.H. Tewari and A.W. McClean: Temperature dependence of point of zero charge of alumina and magnetite. *J. Colloid Interface Sci.* **40,** 267 (1972).
44. N. Marmier, A. Delisee, and F. Fromage: Surface complexation modeling of Yb(III), Ni(II), and Cs(I) sorption on magnetite. *J. Colloid Interface Sci.* **211,** 54 (1999).
45. Z. Cheng, A.V. Geen, C. Jing, X. Meng, A. Seddique, and K.M. Ahmed: Performance of a household-level arsenic removal system during 4-month deployments in Bangladesh. *Environ. Sci. Technol.* **38,** 3442 (2004).
46. X.G. Meng and R.D. Letterman: Effect of component oxide interactions on the adsorption properties of mixed oxides. *Environ. Sci. Technol.* **27,** 970 (1993).
47. F.M.M. Morel and J.G. Hering: *Principles and Applications of Aquatic Chemistry* (Wiley & Sons, New York, 1993).
48. Y. Gao, A.T. Kan, and M.B. Tomson: Critical evaluation of desorption phenomena of heavy metals from natural sediments. *Environ. Sci. Technol.* **37,** 5566 (2003).
49. W. Stumm and J.J. Morgan: *Aquatic Chemistry Chemical Equilibria and Rates in Natural Water,* 2nd ed. (Wiley-Interscience, New York, 1996).
50. A.T. Kan, G. Fu, M. Hunter, W. Chen, C.H. Ward, and M.B. Tomson: Irreversible sorption of neutral hydrocarbons to sediments: Experimental observations and model predictions. *Environ. Sci. Technol.* **32,** 892 (1998).
51. J.A. Munoz, A. Gonzalo, and M. Valiente: Arsenic adsorption by Fe(III)-loaded open-celled cellulose sponge. Thermodynamic and selectivity aspects. *Environ. Sci. Technol.* **36,** 3405 (2002).
52. W.W. Yu, J.C. Falkner, C.T. Yavuz and V.L. Colvin: Synthesis of monodisperse iron oxide nanocrystals by thermal decomposition of iron carboxylate salts. *Chem. Comm.* **20,** 2306 (2004).